# Tumors induce *de novo* steroid biosynthesis in T cells to evade immunity

Bidesh Mahata[1, 2*], Jhuma Pramanik[2], Louise van der Weyden[2], Krzysztof Polanski[2] Gozde Kar[3], Angela Riedel[4], Xi Chen[5], Nuno A. Fonseca[3], Kousik Kundu[2], Lia S. Campos[2], Edward Ryder[2], Graham Duddy[2], Izabela Walczak[2,6], Klaus Okkenhaug[1], David J. Adams[2], Jacqueline D. Shields[4*] and Sarah A. Teichmann[2, 7*]

1. Department of Pathology, University of Cambridge, Cambridge, CB2 1QP, UK
2. Wellcome Sanger Institute, Wellcome Genome Campus, Hinxton, Cambridge, CB10 1SA, UK
3. EMBL-European Bioinformatics Institute, Wellcome Genome Campus, Hinxton, Cambridge, CB10 1SD, UK
4. Medical Research Council Cancer Unit, Hutchison/Medical Research Council Research Centre, Cambridge, UK
5. Department of Biology, Southern University of Science and Technology, Shenzhen, China
6. Iontas Ltd, Iconix Park, Cambridge, CB22 3EG, UK
7. Theory of Condensed Matter, Cavendish Laboratory, 19 JJ Thomson Ave, Cambridge, CB3 0HE, UK

*To whom correspondence should be addressed: st9@sanger.ac.uk, JS970@mrc-cu.cam.ac.uk and bm562@cam.ac.uk

## ABSTRACT

**Tumors subvert immune cell function to evade immune responses, yet the complex mechanisms driving immune evasion remain poorly understood. Here we show that tumors induce *de novo* steroidogenesis in T lymphocytes to evade anti-tumor immunity. Using a novel transgenic steroidogenesis-reporter mouse line we identify and characterize *de novo* steroidogenic immune cells. Genetic ablation of T cell steroidogenesis restricts primary tumor growth and metastatic dissemination in mouse models. Steroidogenic T cells dysregulate anti-tumor immunity, and inhibition of the steroidogenesis pathway was sufficient to restore anti-tumor immunity. This study demonstrates T cell *de novo* steroidogenesis as a mechanism of anti-tumor immunosuppression and a potential druggable target.**

## INTRODUCTION

Steroidogenesis is a metabolic process by which cholesterol is converted to steroids[1]. The biosynthesis of steroids starting from cholesterol is often termed "*de novo* steroidogenesis"[1]. Cytoplasmic cholesterol is transported into the mitochondria, where the rate-limiting enzyme CYP11A1 (also known as P450 side chain cleavage enzyme) converts cholesterol to pregnenolone. Pregnenolone is the first bioactive steroid of the pathway, and the precursor of all other steroids (Figure 1a) [1,2]. The steroidogenesis pathway has been extensively studied in adrenal gland, gonads and placenta. *De novo* steroidogenesis by other tissues, known as "extra-glandular steroidogenesis", in brain[1,3,4], skin[5], thymus[6], and adipose tissues[7] has also been reported. Steroid production as a result of immune response in the mucosal tissues, such as in the lung and intestine, has been shown to play a tolerogenic role to

maintain tissue homeostasis[8,9]. However the physiological and pathological role of extra-glandular steroidogenesis remains largely unknown[2].

In cancer, the immunosuppressive tumor microenviroenmnt (TME) prevents immune cells from mounting an effective anti-tumor immune response[10]. Several mechanisms by which cancer cells evade the immune system have been described[11,12]. These include: (1) immune suppression at the TME mediated by immunosuppressive cells, (2) induction of apoptosis in cytotoxic T lymphocytes (CTLs) by the expression of pro-apoptotic ligands e.g., Fas ligand and TRAIL, (3) dysregulating antigen presentation, (4) release of immunosuppressive factors such as IL-10 and TGFβ, and (5) inducing tolerance and immune deviation by mechanisms including, among others, shifting the balance of Th1 immune responses (type 1 immune response) to Th2 (type 2 immune response), and expression of immune inhibitory molecules such as PD-1 (programmed death-1) and CTLA-4 (CTL antigen-4). Established tumor often show type 2 immune responses that drive a immunocompromised and pro-tumorigenic program[13-16]. Further understanding of the anti-tumor immunosuppression would allow us developing new immunotherapies.

Steroid hormones are known immunosuppressive biomolecules[17,18]. We recently reported that type 2 $CD4^+$ T cells (Th2 lymphocytes) induce *de novo* steroidogenesis to restore immune homeostasis by limiting the immune response against a worm parasite[19]. Thus we sought to determine whether type 2 T cell-mediated steroidogenesis contributes to the generation of a suppressive niche in the TME.

74 To study *de novo* steroidogenesis we generated two novel transgenic mouse lines: a
75 fluorescent reporter mouse line (Cyp11a1-mCherry) and a conditional Cyp11a1
76 (floxed) knockout mouse line. We show the presence of *de novo* steroidogenesis by
77 tumor infiltrating T lymphocytes, but not in unchallenged animals or draining lymph
78 nodes. Genetic ablation of T cell steroidogenesis in Cyp11a1 conditional knockout
79 (cKO) (i.e. *Cyp11a1*$^{fl/fl}$; *Cd4*-Cre) mice restricts experimental primary tumor growth
80 and lung metastasis. We found that intratumoral T cell steroidogenesis dysregulate
81 anti-tumor immunity that could be restored by inhibiting the steroidogenesis pathway
82 pharmacologically. This study therefore demonstrates that T cell *de novo*
83 setroidogenesis is a cause of anti-tumor immunosuppression and a potential drug
84 target for cancer immunotherapy.

85 **RESULTS**

86 **Generation of Cyp11a1-mCherry reporter and Cyp11a1 conditional knockout**
87 **mouse line to study *de novo* steroidogenesis**

88 Cyp11a1 expression is known to be a faithful biomarker of *de novo* steroidogenesis
89 due to its role as a first and rate-limiting enzyme in this pathway[1]. Therefore, we
90 generated a novel reporter mouse line to identify Cyp11a1-expressing steroidogenic
91 cells definitively (Figure 1b, c, Extended Data Figure 1a, b, c and d). As expected,
92 mCherry expression was detected in single cell suspensions of testis and adrenal
93 glands but negligible to no expression in the spleen (Figure 1c) or other tissues
94 including lung, kidney, blood, liver, bone marrow, lymph nodes and thymocytes
95 (Extended Data Figure 1b). However, Cyp11a1-mCherry signal was detected
96 specifically in activated type-2 $CD4^+$ T helper cells (Th2 cells) upon activation *in*
97 *vitro* (Extended Data Figure 1c), as reported previously[19]. Cyp11a1 expression was
98 detectable only in mCherry-expressing T helper cells (Extended Data Figure 1d). To

99 date all Cyp11a1-expressing cells have been found to produce at least one steroid[1].
100 Therefore, we denote Cyp11a1-expressing cells as "*de novo* steroidogenic" or
101 "steroidogenic" cells.
102 To determine the functional consequences of cell type-specific steroidogenesis we
103 created a *Cyp11a1* floxed (*Cyp11a1*$^{fl/fl}$) mouse following EUCOMM/WSI conditional
104 gene targeting strategy[20]. Briefly, a "Knockout-first" (*tm1a*) mouse line was created
105 using a promoter-driven targeting cassette (Figure 1d). The *tm1a* mouse was then
106 crossed with Flp-deleter mice (FlpO) [21] to remove the *LacZ* and *Neo* cassette, and
107 generate a *tm1c* allele (i.e. *Cyp11a1*$^{fl/fl}$). When crossed with a Cre-driver, the Cre-
108 recombinase removes exon 3 of *Cyp11a1* gene and creates a frameshift mutation
109 (Figure 1d). Because we had initially detected Cyp11a1 expression by Th2 cells[19], we
110 crossed the *Cyp11a1*$^{fl/fl}$ line with a *Cd4*-driven Cre-recombinase to delete *Cyp11a1*
111 and prevent *de novo* steroidogenesis in all T cells (Figure 1e). Deletion efficiency of
112 Cre-recombinase in the *Cyp11a1* cKO (*Cd4-Cre;Cyp11a1*$^{fl/fl}$) mice was nearly
113 complete in Th2 cells (Figure 1f). *Cyp11a1* cKO mice showed normal thymic
114 development of T cells, and a normal distribution in the peripheral tissues (Figure 1g,
115 h, i).

116 **Tumors induce functional Cyp11a1 expression in T cells *in vivo***

117 Tumor infiltrating T cells are key fate determinants within a tumor, but are often
118 suppressed[22]. The steroidogenesis-inducing type 2 cytokines such as IL4 are also
119 often present in the TME[23,24], thus we next sought to examine the steroidogenic
120 capacity (i.e. Cyp11a1 induction) of T cells infiltrating tumors, and their impact on
121 tumor development. To explore Cyp11a1 expression *in vivo,* we utilized the well-
122 established B16-F10 melanoma model[25-27] and implanted tumors subcutaneously in
123 *Cyp11a1*-mCherry reporter mice.

124

125 Cyp11a1 expression was detected in immune cells of established primary tumors, but
126 not in tumor-draining brachial lymph nodes (LN) or blood (Figure 2a), indicating that
127 stimulation occurs *in situ*. In support of this, stimulation of splenic and LN resident T
128 cells did not induce Cyp11a1 expression *ex vivo* (Figure 2b, Extended Data figure 2a,
129 LN data not shown). The dominant Cyp11a1$^{+}$ tumor infiltrating immune cells were
130 identified as T cells, predominantly CD4$^{+}$ (helper T cells, Figure 2a). Only a small
131 proportion of the Cyp11a1$^{+}$ cells were reactive to ova, the model antigen in Ova-
132 expressing B16-F10 cells, as determine by staining with MHC-tetramers (Extended
133 Data Figure 2b).

134

135 Having identified presence of Cyp11a1-expressing T cells in established tumors, we
136 next examined expression dynamics during tumor progression. Using the Cyp11a1-
137 mCherry reporter mice we observed an expression of Cyp11a1 in CD4$^{+}$ T cells which
138 remained stable through the development of the tumor through days 7 and 12. By
139 contrast, CD8$^{+}$ T cells only expressed Cyp11a1 by day 12 (Figure 2c, d). Expression
140 dynamics of minor and rare Cyp11a1$^{+}$ non-T cells (mast cell and basophil) is shown
141 in Extended Data Figure 2c, d.

142

143 To determine whether Cyp11a1 induction in T cells is conserved in other tumor types
144 we analyzed a EO771 orthotopic model of breast cancer[28-30] (Figure 2e-g, Extended
145 Data Figure 2e). Again, we found that Cyp11a1 was upregulated in tumor infiltrating
146 T cells (Figure 2e, f, g), but not in tumor draining lymph node or spleen. We also
147 detected minor and rare population of other Cyp11a1$^{+}$ type-2 immune cells, such as
148 mast cells and basophil (Extended Data Figure 2e).

149

150 Next, we sought to measure the functional output of Cyp11a1 expression. Significant
151 concentrations of the steroid pregnenolone were detected exclusively in immune cells
152 isolated from tumors, with negligible levels detected in cells from the spleen (Figure
153 2h). Using the B16-F10 model of experimental metastatic dissemination[31], we
154 determined that lungs with metastatic nodules, but not control lungs without
155 metastatic nodules, had elevated levels of pregnenolone (Figure 2i).

156

157 The presence of tumor cells did not induce or augment the Cyp11a1 expression in T
158 cells *in vitro* (Extended Data Figure 2f). This indicates that type-2 (Th2) cytokines
159 within the TME induce Cyp11a1 expression by T cells and this cannot readily be
160 mimicked *in vitro*.

161

162 Having observed steroidogenic T cells in murine melanoma, we turned to publicly
163 available transcriptomic data sets to verify our findings and ascertain relevance in the
164 human setting. We identified *CYP11A1* mRNA expression, and thus steroidogenic
165 potential, in a range of cancer types including liver, breast, prostate, lung, kidney,
166 sarcoma, glioma, uterine, cervical, lymphoma and melanoma (Figure 2j and Extended
167 Data Figure 2g, h)[24]. Human melanoma tissues represented a prominent steroidogenic
168 tumor type, expressing *CYP11A1, HSD3B1, HSD3B2, CYP17A1, CYP21A1,*
169 *CYP11B1* and not expressing *CYP11B2* (Figure 2k). Together this was indicative of
170 melanoma-driven production of glucocorticoids (Figure 2k, Extended Data Figure 2i).

171

172 Interestingly, in melanoma, steroidogenic gene expression was correlated with *IL4*
173 expression (Figure 2k, Extended Data Figure 2j), a key inducer of T cell

174 steroidogenesis[19]. Moreover, analysis of human tumor infiltrating $CD4^+$ T cell
175 transcriptomes, confirmed *CYP11A1* expression (Figure 2l) implying that $CD4^+$ T
176 cells are a source of steroids in tumors, mirroring the murine setting. Collectively
177 these data indicate that TILs produce steroids within the tumor both in human and
178 mouse.
179
180 **Ablation of T cell de novo steroidogenesis restricts experimental tumor growth**
181 **and metastasis**
182 To determine the functional consequences of T cell-driven steroidogenesis in tumors
183 we subcutaneously implanted *Cyp11a1* cKO mice with B16-F10 cells. Genetic
184 deletion of *Cyp11a1* in T cells significantly restricted primary tumor growth rates and
185 final volumes (Figure 3a). Similarly, in the experimental metastasis model, impaired
186 lung colonization was observed in the absence of T cell-expressed Cyp11a1. There
187 was a significant reduction in number of metastatic foci in lungs of *Cyp11a1* cKO
188 mice compared to the control mice (Figure 3b). In the B16-F10 subcutaneous
189 melanoma model, topical application of exogenous pregnenolone at the primary
190 tumor site was sufficient to compensate for the Cyp11a1 deficiency, restoring tumor
191 growth to levels comparable with control mice (Figure 3c). This suggests that the
192 tumor restriction was a consequence of the absence of pregnenolone synthesis.
193 Similar results were obtained using the EO771 breast cancer orthotopic tumor model:
194 deletion of *Cyp11a1* in T cells restricted dissemination to and nodule formation in the
195 lung (Figure 3d). Importantly, in both tumor models, pharmacological inhibition of
196 Cyp11a1 by aminoglutethimide (AG) was sufficient to recapitulate the tumor
197 restriction phenotype resulting from *Cyp11a1* genetic ablation (Figure 3e, f).
198 Together, these data indicate that, T cell-derived steroids can support tumor growth

199 and both genetic and pharmacological interference with the pathway can restrict
200 tumor growth.
201
202 **Inhibition of T cell steroidogenesis stimulates anti-tumor immunity**
203 Steroid hormones can induce an immunosuppressive M2-like phenotype in
204 macrophages[17,32,33] cell death and anergy in T cells[17 34-36], tolerance in dendritic
205 cells[17,37-39] and increase the frequency of Treg cells[40-42]. Therefore, we tested whether
206 steroidogenic T cells support tumor growth through the induction of
207 immunosuppressive phenotypes in infiltrating immune cells. To determine whether
208 intratumoral macrophages were M1 or M2 type, we purified tumor infiltrating
209 macrophages and analyzed mRNA expression of the M2-macrophage signature genes
210 *Arg1* and *Tgfb1*. In tumor-infiltrating macrophages from *Cyp11a1* cKO mice, *Arg1*
211 and *Tgfb1* mRNA expression was significantly reduced compared to the control mice,
212 indicating fewer of the tumor-supporting M2 macrophages in the T cell-specific
213 *Cyp11a1* knockout mice (Figure 4a). We confirmed changes in macrophage
214 characteristics at the protein level, showing a significant decrease in $Arg1^+$
215 macrophages (M2) with coincident increase in tumor infiltrating $iNOS^+$ macrophages
216 (M1) upon T cell-specific *Cyp11a1* deletion (Figure 4b, c). Hence, depletion of
217 Cyp11a1 in T cells increases the M1/M2 macrophage ratio in the TME.
218
219 Consistent with enhanced tumor immunity, we found significantly higher levels of
220 the inflammatory cytokines *Ifng* and *Tnfa* expression were identified in $CD8^+$ T cells
221 following *Cyp11a1* ablation (Figure 4d). Moreover the expression of the co-inhibitory
222 receptors[43-45] PD1 and TIGIT on tumor-infiltrating T cells was reduced in $CD4^+$ TILs
223 in the *Cyp11a1* cKO mice compared with control littermates (Extended Data Figure

224 3a). The data indicate greater T cell functionality and less exhaustion in the *Cyp11a1*
225 cKO mice.
226
227 To test cytotoxic capacity of T and NK cell populations, we examined the
228 degranulation response of these cells by analyzing cell surface expression of
229 CD107a/LAMP1 in tumor-infiltrating T and NK cells. We observed a significantly
230 increased proportion of degranulating $CD107a^{+}CD8^{+}$ T cells in *Cyp11a1* cKO mice
231 compared to control mice (Figure 4e). The degranulation response in NK cells and
232 $CD4^{+}$ T cells was also enhanced (Figure 4f, g).
233
234 Finally, we observed that proportion of intratumoral Tregs was decreased (Figure 4h).
235 Altogether these data suggest that inhibition of T cell steroidogenesis by genetic
236 deletion of *Cyp11a1* changes the immune cell composition in the tumor
237 microenvironment in favour of anti-tumor immunity.
238
239 Similar to the genetic deletion of *Cyp11a1*, application of the Cyp11a1 inhibitor
240 aminoglutethimide significantly increased frequencies of M1 macrophages and
241 degranulating T and NK cells (Figure 4i, j, k, l, Extended Data Figure 3b)
242 recapitulating anti-tumor phenotypes. *Cyp11a1* inhibition also decreased the number
243 of M2 macrophages in the tumor (Figure 4i). Together, these data demonstrate the
244 potential to stimulate anti-tumor immunity through pharmacological suppression of
245 *Cyp11a1*-dependent steroidogenesis pathways.
246
247 **DISCUSSION**

248 The endocrine importance of systemic steroid hormones is well documented in
249 regulating cell metabolism and immune cell function but the intracrine, autocrine and
250 paracrine role of local cell type specific steroidogenesis is less clear, particularly in
251 pathologies such as cancer[1,2]. This is in part due to the lack of tools to study
252 steroidogenesis in a tissue-specific manner *in vivo*. To overcome this, we generated a
253 novel *Cyp11a1*-mCherry reporter and a conditional *Cyp11a1* knockout mouse strain
254 to identify *de novo* steroidogenic cells and study their role *in vivo*. Using these
255 discovery tools, complemented by pharmacological intervention, we uncovered a
256 novel anti-tumor immune suppression mechanism that may be exploited clinically to
257 boost the anti-tumor immunity (Figure 5).
258
259 The TME harbors innate immune cells such as macrophages, neutrophils, eosinophils,
260 mast cells, myeloid derived suppressor cells, dendritic cells, and natural killer cells,
261 adaptive immune cells such as T and B cells, stromal cells such as fibroblasts,
262 endothelial cells, pericytes, mesenchymal cells, and cancer cells. The presence of
263 immune cells in the tumor microenvironment raised a long-standing question: How
264 tumors evade the immune surveillance and anti-tumor immunity? The present
265 understanding suggests that the balance between protective anti-tumoral immune cells
266 (and other protective factors) and pro-tumoral immunosuppressive cells (and other
267 immunosuppressive factors) determines the fate. Anti-tumoral immune cell subsets
268 includes Th1, Tc1 ($CD8^+$ CTL), M1 macrophage, DC1 which are antagonized by
269 Th2, M2, tolerogenic DC, immature DC, DC2, Treg and myeloid derived suppressor
270 cells. Established tumors are often foster immunosuppressive and tolerogenic immune
271 cells. In this report, the discovery of immune cell-mediated steroid biosynthesis in the
272 TME explains beautifully how immunosuppressive TME can be achieved. Previously

273 it has been shown in several independent reports that steroids induce anergy and cell
274 death in T cells[34-36,46], M2 phenotype in macrophages[32,33], tolerance in DCs[37-39] and
275 increase the frequency of Treg cells[40-42]. Here we demonstrate that tumor infiltrating
276 T cells can produce steroids and that the inhibition of T cell-mediated steroid
277 biosynthesis tips the balance toward protective immunity. Importantly, this pathway
278 can be targeted pharmacologically. This may be exploited therapeutically in three
279 ways: (1) steroidogenic gene expression or the presence of steroids might be used to
280 stratify the patients (2) use of pharmacologic drug (i.e. anti-steroidogenic) can convert
281 the TME into protective type-1 inflammatory condition by reducing the steroid level
282 and (3) immunotherapy should work better in absence of immunosuppressive steroids.
283
284 We identified three distinct classes of immune cells with steroidogenic potential, T
285 cells (Th2 and Tc2, major population), mast cell (rare and minor population), basophil
286 (rare and minor population) and a few monocyte/macrophage. T cells outnumbered
287 other types of Cyp11a1-expressing cells. This explains why deletion of Cyp11a1 in T
288 cells significantly reduced steroidogenesis and its effect. The presence of Cyp11a1$^{+}$
289 non-T cells indicates that in a different context such as in different tumor types the
290 steroidogenic population may vary. Depending upon the immunologic context and
291 congressing of tumor associated cell types the intratumoral steroid pool may vary and
292 play role beyond the immune suppression. For example, synthesis of estrogen,
293 progesterone or androgen may have direct effect on cancer cell survival and
294 proliferation, immunogenicity and that may impose another level of concern because
295 breast, prostate and endometrial cancer are steroid sensitive and constitute a large
296 fraction of all cancer occurrence [47-49]. Previously it was reported that intratumoral *de*
297 *novo* steroidogenesis promotes post-castration prostate cancer growth[50]. Though the

298 role of immune cells in this context is unexplored. Future studies are essential to get
299 detailed insight of immune cell-mediated intratumoral steroidogenesis in each tumor
300 types.
301
302 The study strongly supports the concern raised by recent studies about proper use of
303 steroids, particularly glucocorticoids, in solid tumors as a part of the disease
304 management, specifically when we seek to boost anti-tumor immune response[51-58].
305 Glucocorticoids have been used in clinical oncology for over a half a century, and at
306 present these are routinely used to alleviate edema in patients with intracranial lesions
307 and are first-line agents to suppress immune-related adverse events that arise with the
308 immunotherapies. Therefore, further studies are required to evaluate the use of
309 synthetic steroids when the tumors itself induces glucocorticoid synthesis. Reduction
310 of intratumoral steroidogenesis may open a window for immunotherapies to work
311 better at lower doses.
312
313 Similar experimental approaches can in future provide in depth mechanistic insights
314 into other extraglandular (local) steroidogenic cell types such as adipose cells, neuron,
315 osteoblasts, astrocytes, microglia, skin, trophoblast and thymic epithelial cells. Our
316 *Cyp11a1*-mCherry reporter mouse line can be used as a discovery tool to identify new
317 steroidogenic cell types in tolerogenic physiological conditions such as pregnancy,
318 mucosal tolerance, and inflammatory and immunopathological conditions. Their
319 functional role can be dissected by using *Cyp11a1* cKO mice using tissue specific
320 Cre-drivers. Nevertheless, cancer is a proven context where tumors hijack this
321 pathway for immune evasion. Further studies in diverse physiological scenarios

322 would be of great interest to more broadly understand the role of immune cell *de novo*
323 steroidogenesis in regulating inflammation and immunity.
324
325 **Materials and Methods**
326 *Mice*
327 The care and use of all mice in this study were in accordance with the UK Animals in
328 Science Regulation Unit's Code of Practice for the Housing and Care of Animals
329 Bred, Supplied or Used for Scientific Purposes, the Animals (Scientific Procedures)
330 Act 1986 Amendment Regulations 2012. All procedures were performed under a UK
331 Home Office Project license (PPL 80/2574 or PPL P8837835 or PPL P6B8058B0),
332 which was reviewed and approved by the local institute's Animal Welfare and Ethical
333 Review Body.
334
335 *Generation of a Cyp11a1-mCherry reporter mouse line*
336 *Targeting Description:* Using CRISPR_Cas9 (Clustered Regularly Interspaced Short
337 Palindromic Repeats) [59] technology we introduced double strand DNA breaks 5' and
338 3' adjacent to the *Cyp11a1* termination codon in exon 9 to facilitate the introduction
339 of our targeting construct. The 5' and 3' arms of homology were designed to remove
340 the *Cyp11a1* termination codon and 100bp of the 3' UTR immediately downstream
341 and replace it with a minimal T2a self-cleavage peptide followed by the fluorescent
342 marker mCherry.
343
344 *Cyp11a1 Guide RNA generation and ESC targeting.*
345 *sgRNA design and cloning:* Using the web-based tool designed by Hodgkins et al[60],
346 two sgRNAs were identified 5' and 3' adjacent to the Cyp11a1 termination codon.

347 The guide sequences were ordered from Sigma Genosys as sense and antisense
348 oligonucleotides, and annealed before individually cloning into the human U6 (hU6)
349 expression plasmid (kind gift from Sebastian Gerety).
350
351 *Targeted ES cell generation*: $3x10^6$ C57Bl/6 JM8 ESC (kind gift from Bill Skarnes)
352 were nucleofected with 2ugs *Cyp11a1* circular targeting construct, 1.5ugs of each
353 hU6_sgRNAs and 3ugs a plasmid expressing human codon-optimised CAS9 driven
354 by the CMV promotor (Addgene # 41815). 48 hours post transfection the media was
355 changed for G418 selection media. Confirmation of the correct targeting events were
356 confirmed by qPCR for loss of heterozygosity (LOH) and the presence of the
357 selectable marker, and long range (LR) PCR and Sanger sequencing.
358
359 *Breeding and removal of the Selectable marker:* Following blastocyst injection and
360 chimaera breeding three F1 Cyp11a1+/$^{mCherry\text{-}Neo}$ mice were breed to pCAGGSs-Flpo
361 (kind gift from Andrea Kranz )[21] mice to remove the neomycin selectable marker to
362 generate Cyp11a1$^{+/mCherry}$.
363
364 *Generation of a Cyp11a1 cKO mice*
365 *Cyp11a1$^{fl/fl}$* mice were generated by crossing Cyp11a1$^{tm1a(KOMP)Wtsi}$ mice with a
366 previously reported Flp-deleter (FlpO) line[21]. *Cyp11a1$^{fl/fl}$* mice were crossed with
367 *Cd4-cre* mice to generate the *Cyp11a1* cKO mice.
368
369 *Syngeneic melanoma model*
370 B16-F10 melanoma model: The C57BL/6 derived B16-F10 melanoma cell line was
371 purchased from American Type Culture Collection (ATCC) and cultured in

372 Dulbecco's Modified Eagle medium (DMEM, Life Technologies), supplemented with
373 Penstrep and 10% FBS. For the primary tumor growth assay, 2.5 x$10^5$ B16-F10 cells
374 were injected subcutaneously into the shoulders of either wild type (WT) C57BL/6
375 mice, *Cd4-Cre, Cyp11a1*$^{fl/fl}$ or *Cd4-Cre;Cyp11a1*$^{fl/fl}$ mice. After 11 or 12 days animals
376 were sacrificed and tissues collected for analysis. For the experimental metastasis
377 assay, 5×$10^5$ B16-F10 cells in a volume of 0.1 ml PBS were injected intra-venously
378 into the tail vein. After ten days (±1 day) the mice were sacrificed *via* cervical
379 dislocation, and their lungs removed and rinsed in phosphate buffered saline. The
380 number of B16-F10 colonies on all five lobes of the lung were counted
381 macroscopically.
382 Orthotopic EO771 (Synonym E0771) breast cancer model: The EO771 breast cancer
383 cell line was purchased from CH3 BioSystems and cultured in RPMI (Sigma)
384 supplemented with 10% FBS, 1% PS and 10mM HEPES. 2.5 x$10^5$ cells were injected
385 into the 4th inguinal mammary fat pad of Cyp11a1-mCherry reporter mice. Tumors
386 and inguinal lymph node were collected after 15 days of tumor development.
387 Lung colonization of EO771 cells: EO771 cells were kindly gifted by Robin
388 Anderson. X $10^5$ cells were injected intra-venously in to the tail vein. After ten days
389 (±1 day) the mice were sacrificed via cervical dislocation, and their lungs were
390 removed, ringed in PBS and fixed in . The fixed lungs were sectioned and stained
391 with Hematoxylin and Eosin using professional service. The microscopic image were
392 captured in Olympus with 10X magnification and area of the lung tumours were
393 measured by ImageJ.
394
395 *Tumor Tissue Processing*

396 Tumors were mechanically dissociated and digested in 1mg/ml collagenase D
397 (Roche), 1mg/ml collagenase A (Roche) and 0.4mg/ml DNase I (Sigma) in IMDM
398 media containing 10% FBS, at 37°C for 40 mins. EDTA was added to all samples to
399 neutralize collagenase activity (final concentration 5mM) and digested tissues were
400 passed through 70µm filters (Falcon).
401
402 *Cell sorting*
403 Once processed, single cell suspension tumour samples were incubated with a fixable
404 fluorescent viability stain (Life Technologies) for 20mins (diluted 1:1000 in PBS)
405 prior to incubation with conjugated primary antibodies for 30 mins at $4^0$C. Antibodies
406 were diluted in PBS 0.5% BSA. Stained samples were sorted, using the MoFlo XDP
407 or BD Influx cytometer system.
408
409 *B16-F10 and T cell co-culture assay*
410 Negatively purified splenic naïve $CD4^+$ T cells from Cyp11a1-mCherry mice were
411 cultured in presence of B16-F10 cell with or without TCR activation and analyzed by
412 flow cytometry to detect Cyp11a1-mCherry expression. Naïve T cell purification and
413 activation condition is described previously[61]. Briefly, naïve splenic cells were
414 activated in anti-CD3e and anti-CD28 coated plate in presence of IL2 but in absence
415 anti-IL4 neutralizing antibody.
416
417 *Quantitative PCR (qPCR)*
418 Tumor infiltrating macrophages ($Lin^-CD11b^+$) and $CD8^+$ T cells were purified by cell
419 sorting. We used the Cells-to-$C_T$ kit (Invitrogen/Thermofisher Scientific) and
420 followed SYBR Green format according to manufacturer's instructions. 2µl of cDNA

421 was used in 12µl qPCR reactions with appropriate primers and SYBR Green PCR
422 Master Mix (Applied Biosystems). Data were analyzed by ddCT method.
423 Experiments were performed 3 times and data represent mean values ± standard
424 deviation. The primer list is provided below:

425 *Arg1*: F- ATGGAAGAGACCTTCAGCTAC
426 R- GCTGTCTTCCCAAGAGTTGGG
427 *Tgfβ1*: F- TGACGTCACTGGAGTTGTACGG
428 R- GGTTCATGTCATGGATGGTGC
429 *Ifnγ*: F- ACAATGAACGCTACACACTGC
430 R- CTTCCACATCTATGCCACTTGAG;
431 *Tnfα*: F- CATCTTCTCAAAATTCGAGTGACAA
432 R- TGGGAGTAGACAAGGTACAACCC
433 *Gapdh*: F- ACCACAGTCCATGCCATCAC
434 R- GCCTGCTTCACCACCTTC
435 *Rplp0*: F: CACTGGTCTAGGACCCGAGAA
436 R: GGTGCCTCTGGAGATTTTCG

437 *Flow cytometry*

438 We followed eBioscience surface staining, intracellular cytotoplasmic protein staining
439 (for cytokines) protocols. Briefly, single cell suspension was stained with Live/Dead
440 Fixable Dead cell stain kit (Molecular Probes/ Thermo Fisher) and blocked by
441 purified rat anti-mouse CD16/CD32 purchased from BD Bioscience and eBioscience.
442 Surface staining was performed in flow cytometry staining buffer (eBioscience) or in
443 PBS containing 3% FCS at $4^0$C. For intracellular cytokine staining cells were fixed by
444 eBioscience IC Fixation buffer and permeabililzed by eBioscience permeabilization
445 buffer. Cells were stained in 1x permeabilization buffer with fluorescent dye-

446 conjugated antibodies. After staining cells were washed with flow cytometry staining
447 buffer (eBioscience) or 3% PBS-FCS, and were analyzed by flow cytometer Fortessa
448 (BD Biosciences) using FACSDiva. The data were analyzed by FlowJo software.
449 Antibodies used in flow cytometry were: CD4 (RM4-5 or GK1.5), CD8a (53-6.7),
450 CD3e (145-2c11), CD45 (30F11), CD44 (IM7), CD25 (PC61), B220 (Ra3-6b2),
451 Cyp11a1 (C-16, unconjugated, Santa Cruz; Fluorescent dye conjugated anti-goat
452 secondary was used for staining), Ly6G (1A8), Ly6G/Ly6C (Gr-1) (RB6-8C5), Ly6C
453 (HK1.4), CD11b (M1/70), CD11c (N418), CD19 (1D3), NK1.1(Pk136), Ter119
454 (TER119), PD-1 (J43), TIGIT (1G9), CD107a/LAMP1(1D4B). All antibodies were
455 purchased from eBioscience, BD Bioscience or Biolegend.
456
457 *Western Blot Antibodies*
458 Anti-CYP11A1 (Santa Cruz Biotechnology, C-16) and anti-TBP (Abcam) were used.
459
460 *Quantitative ELISA*
461 $CD45^+$ leukocytes were purified from B16-F10 tumor masses and lungs, of mice that
462 had been tail vein administered B16-F0 cells, and seeded at equal density in IMDM
463 medium supplemented with 10% charcoal stripped fetal bovine serum (Life
464 Technologies, Invitrogen) for 24 hrs. Pregnenolone concentrations of the culture
465 supernatants were quantified using pregnenolone ELISA kit (Abnova) and
466 corticosteroids ELISA (Thermofisher) kit following manufacturers' instruction.
467 Absorbance was measured at 450 nm, and data were analyzed in GraphPad Prism 5.
468 *B16-F10 and T cell co-culture assay*

469 Negatively purified splenic naïve $CD4^+$ T cells from Cyp11a1-mCherry mice were
470 cultured in presence of B16-F10 cell with or without TCR activation and analyzed by
471 flow cytometry to detect Cyp11a1-mCherry expression.
472

473 **Acknowledgements**
474 We would like to thank Ana C. Anderson and Rahul Roychoudhuri for their valuable
475 comments on the manuscript and useful discussions; Jana Eliasova and Sarah
476 Davidson for her help with diagram illustration; Bee Ling Ng, Chris Hall, Sam
477 Thompson and Jennie Graham for help with flow cytometry and cell sorting;
478 Research Support Facility, WSI, for their technical help and animal husbandry.
479 EO771 cells were kindly gifted by Robin Anderson.
480 **Funding**
481 CRUK Cancer Immunology fund (Ref. 20193), ERC consolidator grant (ThDEFINE,
482 Project ID: 646794) and Wellcome Sanger Institute core funding (WT206194)
483 supported this study.
484 **Author contribution**
485 BM: Led and managed the project, generated hypothesis, designed and performed
486 experiments, analyzed data, and wrote manuscript JP: Performed experiments,
487 analyzed data and helped in genetically modified mouse generation. LvdW:
488 Performed B16-F10 and EO771 pulmonary metastasis experiments, analyzed data.
489 AR: Performed B16-F10 subcutaneous tumors experiments, analyzed data. GK, NAF
490 and KK: Analyzed publicly available gene expression datasets to confirm human
491 tumor expression of steroidogenic genes. LSC: Helped in identification and
492 quantification of tumor spots in EO771 lung metastasis. ER and GD: Helped in
493 generation of *Cyp11a*-mCherry and *Cyp111a1*$^{fl/fl}$ mouse model. IW: Built the

494 *Cyp11a1*-mCherry targeting construct. KO: Helped in designing experiments, writing
495 manuscript, critical comments and supervision. DJA: Conducted pulmonary
496 metastasis experiments. JS: Conducted B16-F10 subcutaneous experiments under her
497 PPL and supervised the study. SAT: Supervised the study. All authors commented on
498 and approved of the draft manuscript before submission.

499

500 **REFERENCES**


501 1 Miller, W. L. & Auchus, R. J. The molecular biology, biochemistry, and physiology of human
502 steroidogenesis and its disorders. *Endocr Rev* **32**, 81-151, doi:10.1210/er.2010-0013 (2011).
503 2 Miller, W. L. Steroidogenesis: Unanswered Questions. *Trends in endocrinology and*
504 *metabolism: TEM* **28**, 771-793, doi:10.1016/j.tem.2017.09.002 (2017).
505 3 Belelli, D. & Lambert, J. J. Neurosteroids: endogenous regulators of the GABA(A) receptor.
506 *Nature reviews. Neuroscience* **6**, 565-575, doi:10.1038/nrn1703 (2005).
507 4 Hosie, A. M., Wilkins, M. E., da Silva, H. M. & Smart, T. G. Endogenous neurosteroids
508 regulate GABAA receptors through two discrete transmembrane sites. *Nature* **444**, 486-489,
509 doi:10.1038/nature05324 (2006).
510 5 Slominski, A. *et al*. Steroidogenesis in the skin: implications for local immune functions. *The*
511 *Journal of steroid biochemistry and molecular biology* **137**, 107-123,
512 doi:10.1016/j.jsbmb.2013.02.006 (2013).
513 6 Vacchio, M. S., Papadopoulos, V. & Ashwell, J. D. Steroid production in the thymus:
514 implications for thymocyte selection. *The Journal of experimental medicine* **179**, 1835-1846
515 (1994).
516 7 Li, J., Papadopoulos, V. & Vihma, V. Steroid biosynthesis in adipose tissue. *Steroids* **103**, 89-
517 104, doi:10.1016/j.steroids.2015.03.016 (2015).
518 8 Cima, I. *et al*. Intestinal epithelial cells synthesize glucocorticoids and regulate T cell
519 activation. *The Journal of experimental medicine* **200**, 1635-1646, doi:10.1084/jem.20031958
520 (2004).
521 9 Hostettler, N. *et al*. Local glucocorticoid production in the mouse lung is induced by immune
522 cell stimulation. *Allergy* **67**, 227-234, doi:10.1111/j.1398-9995.2011.02749.x (2012).
523 10 Hanahan, D. & Weinberg, R. A. Hallmarks of cancer: the next generation. *Cell* **144**, 646-674,
524 doi:10.1016/j.cell.2011.02.013 (2011).
525 11 Vinay, D. S. *et al*. Immune evasion in cancer: Mechanistic basis and therapeutic strategies.
526 *Semin Cancer Biol* **35 Suppl**, S185-S198, doi:10.1016/j.semcancer.2015.03.004 (2015).
527 12 Beatty, G. L. & Gladney, W. L. Immune escape mechanisms as a guide for cancer
528 immunotherapy. *Clin Cancer Res* **21**, 687-692, doi:10.1158/1078-0432.CCR-14-1860 (2015).
529 13 DeNardo, D. G. *et al*. CD4(+) T cells regulate pulmonary metastasis of mammary carcinomas
530 by enhancing protumor properties of macrophages. *Cancer Cell* **16**, 91-102,
531 doi:10.1016/j.ccr.2009.06.018 (2009).
532 14 Kobayashi, M., Kobayashi, H., Pollard, R. B. & Suzuki, F. A pathogenic role of Th2 cells and
533 their cytokine products on the pulmonary metastasis of murine B16 melanoma. *J Immunol*
534 **160**, 5869-5873 (1998).
535 15 De Monte, L. *et al*. Intratumor T helper type 2 cell infiltrate correlates with cancer-associated
536 fibroblast thymic stromal lymphopoietin production and reduced survival in pancreatic cancer.
537 *J Exp Med* **208**, 469-478, doi:10.1084/jem.20101876 (2011).
538 16 Hanahan, D. & Coussens, L. M. Accessories to the crime: functions of cells recruited to the
539 tumor microenvironment. *Cancer Cell* **21**, 309-322, doi:10.1016/j.ccr.2012.02.022 (2012).
540 17 Cain, D. W. & Cidlowski, J. A. Immune regulation by glucocorticoids. *Nature reviews.*
541 *Immunology* **17**, 233-247, doi:10.1038/nri.2017.1 (2017).
542 18 Klein, S. L. & Flanagan, K. L. Sex differences in immune responses. *Nature reviews.*
543 *Immunology* **16**, 626-638, doi:10.1038/nri.2016.90 (2016).

19 Mahata, B. *et al*. Single-cell RNA sequencing reveals T helper cells synthesizing steroids de novo to contribute to immune homeostasis. *Cell Rep* **7**, 1130-1142, doi:10.1016/j.celrep.2014.04.011 (2014).
20 Skarnes, W. C. *et al*. A conditional knockout resource for the genome-wide study of mouse gene function. *Nature* **474**, 337-342, doi:10.1038/nature10163 (2011).
21 Kranz, A. *et al*. An improved Flp deleter mouse in C57Bl/6 based on Flpo recombinase. *Genesis* **48**, 512-520, doi:10.1002/dvg.20641 (2010).
22 Mellman, I., Coukos, G. & Dranoff, G. Cancer immunotherapy comes of age. *Nature* **480**, 480-489, doi:10.1038/nature10673 (2011).
23 Landskron, G., De la Fuente, M., Thuwajit, P., Thuwajit, C. & Hermoso, M. A. Chronic inflammation and cytokines in the tumor microenvironment. *Journal of immunology research* **2014**, 149185, doi:10.1155/2014/149185 (2014).
24 Papatheodorou, I. *et al*. Expression Atlas: gene and protein expression across multiple studies and organisms. *Nucleic acids research* **46**, D246-D251, doi:10.1093/nar/gkx1158 (2018).
25 Curran, M. A., Montalvo, W., Yagita, H. & Allison, J. P. PD-1 and CTLA-4 combination blockade expands infiltrating T cells and reduces regulatory T and myeloid cells within B16 melanoma tumors. *Proceedings of the National Academy of Sciences of the United States of America* **107**, 4275-4280, doi:10.1073/pnas.0915174107 (2010).
26 De Henau, O. *et al*. Overcoming resistance to checkpoint blockade therapy by targeting PI3Kgamma in myeloid cells. *Nature* **539**, 443-447, doi:10.1038/nature20554 (2016).
27 Zamarin, D. *et al*. Intratumoral modulation of the inducible co-stimulator ICOS by recombinant oncolytic virus promotes systemic anti-tumour immunity. *Nature communications* **8**, 14340, doi:10.1038/ncomms14340 (2017).
28 Kisielow, J., Obermair, F. J. & Kopf, M. Deciphering CD4(+) T cell specificity using novel MHC-TCR chimeric receptors. *Nat Immunol* **20**, 652-662, doi:10.1038/s41590-019-0335-z (2019).
29 Casey, A. E., Laster, W. R., Jr. & Ross, G. L. Sustained enhanced growth of carcinoma EO771 in C57 black mice. *Proc Soc Exp Biol Med* **77**, 358-362, doi:10.3181/00379727-77-18779 (1951).
30 Johnstone, C. N. *et al*. Functional and molecular characterisation of EO771.LMB tumours, a new C57BL/6-mouse-derived model of spontaneously metastatic mammary cancer. *Dis Model Mech* **8**, 237-251, doi:10.1242/dmm.017830 (2015).
31 van der Weyden, L. *et al*. Genome-wide in vivo screen identifies novel host regulators of metastatic colonization. *Nature* **541**, 233-236, doi:10.1038/nature20792 (2017).
32 Martinez, F. O. & Gordon, S. The M1 and M2 paradigm of macrophage activation: time for reassessment. *F1000Prime Rep* **6**, 13, doi:10.12703/P6-13 (2014).
33 Roszer, T. Understanding the Mysterious M2 Macrophage through Activation Markers and Effector Mechanisms. *Mediators Inflamm* **2015**, 816460, doi:10.1155/2015/816460 (2015).
34 Desbarats, J., You-Ten, K. E. & Lapp, W. S. Levels of p56lck and p59fyn are reduced by a glucocorticoid-dependent mechanism in graft-versus-host reaction-induced T cell anergy. *Cell Immunol* **163**, 10-18, doi:10.1006/cimm.1995.1093 (1995).
35 Van Laethem, F. *et al*. Glucocorticoids attenuate T cell receptor signaling. *J Exp Med* **193**, 803-814, doi:10.1084/jem.193.7.803 (2001).
36 Heijink, I. H. & Van Oosterhout, A. J. Strategies for targeting T-cells in allergic diseases and asthma. *Pharmacol Ther* **112**, 489-500, doi:10.1016/j.pharmthera.2006.05.005 (2006).
37 Gordon, J. R., Ma, Y., Churchman, L., Gordon, S. A. & Dawicki, W. Regulatory dendritic cells for immunotherapy in immunologic diseases. *Front Immunol* **5**, 7, doi:10.3389/fimmu.2014.00007 (2014).
38 Piemonti, L. *et al*. Glucocorticoids affect human dendritic cell differentiation and maturation. *J Immunol* **162**, 6473-6481 (1999).
39 Woltman, A. M. *et al*. The effect of calcineurin inhibitors and corticosteroids on the differentiation of human dendritic cells. *Eur J Immunol* **30**, 1807-1812, doi:10.1002/1521-4141(200007)30:7<1807::AID-IMMU1807>3.0.CO;2-N (2000).
40 Chen, X., Oppenheim, J. J., Winkler-Pickett, R. T., Ortaldo, J. R. & Howard, O. M. Glucocorticoid amplifies IL-2-dependent expansion of functional FoxP3(+)CD4(+)CD25(+) T regulatory cells in vivo and enhances their capacity to suppress EAE. *Eur J Immunol* **36**, 2139-2149, doi:10.1002/eji.200635873 (2006).
41 Hu, Y. *et al*. Function of regulatory T-cells improved by dexamethasone in Graves' disease. *Eur J Endocrinol* **166**, 641-646, doi:10.1530/EJE-11-0879 (2012).

42 Suarez, A., Lopez, P., Gomez, J. & Gutierrez, C. Enrichment of CD4+ CD25high T cell population in patients with systemic lupus erythematosus treated with glucocorticoids. *Ann Rheum Dis* **65**, 1512-1517, doi:10.1136/ard.2005.049924 (2006).

43 Sakuishi, K. *et al*. Targeting Tim-3 and PD-1 pathways to reverse T cell exhaustion and restore anti-tumor immunity. *The Journal of experimental medicine* **207**, 2187-2194, doi:10.1084/jem.20100643 (2010).

44 Anderson, A. C., Joller, N. & Kuchroo, V. K. Lag-3, Tim-3, and TIGIT: Co-inhibitory Receptors with Specialized Functions in Immune Regulation. *Immunity* **44**, 989-1004, doi:10.1016/j.immuni.2016.05.001 (2016).

45 Chihara, N. *et al*. Induction and transcriptional regulation of the co-inhibitory gene module in T cells. *Nature* **558**, 454-459, doi:10.1038/s41586-018-0206-z (2018).

46 Rhen, T. & Cidlowski, J. A. Antiinflammatory action of glucocorticoids--new mechanisms for old drugs. *N Engl J Med* **353**, 1711-1723, doi:10.1056/NEJMra050541 (2005).

47 DeVita, V. T., Lawrence, T. S. & Rosenberg, S. A. *DeVita, Hellman, and Rosenberg's cancer : principles & practice of oncology*. 11th edition. edn, (Wolters Kluwer, 2019).

48 Risbridger, G. P., Davis, I. D., Birrell, S. N. & Tilley, W. D. Breast and prostate cancer: more similar than different. *Nat Rev Cancer* **10**, 205-212, doi:10.1038/nrc2795 (2010).

49 Salmon, H., Remark, R., Gnjatic, S. & Merad, M. Host tissue determinants of tumour immunity. *Nat Rev Cancer* **19**, 215-227, doi:10.1038/s41568-019-0125-9 (2019).

50 Locke, J. A. *et al*. Androgen levels increase by intratumoral de novo steroidogenesis during progression of castration-resistant prostate cancer. *Cancer Res* **68**, 6407-6415, doi:10.1158/0008-5472.CAN-07-5997 (2008).

51 Flint, T. R. *et al*. Tumor-Induced IL-6 Reprograms Host Metabolism to Suppress Anti-tumor Immunity. *Cell Metab* **24**, 672-684, doi:10.1016/j.cmet.2016.10.010 (2016).

52 Connell, C. M. *et al*. Cancer immunotherapy trial registrations increase exponentially but chronic immunosuppressive glucocorticoid therapy may compromise outcomes. *Ann Oncol* **28**, 1678-1679, doi:10.1093/annonc/mdx181 (2017).

53 Della Corte, C. M. & Morgillo, F. Early use of steroids affects immune cells and impairs immunotherapy efficacy. *ESMO Open* **4**, e000477, doi:10.1136/esmoopen-2018-000477 (2019).

54 Draghi, A. *et al*. Differential effects of corticosteroids and anti-TNF on tumor-specific immune responses: implications for the management of irAEs. *Int J Cancer* **145**, 1408-1413, doi:10.1002/ijc.32080 (2019).

55 Obradovic, M. M. S. *et al*. Glucocorticoids promote breast cancer metastasis. *Nature* **567**, 540-544, doi:10.1038/s41586-019-1019-4 (2019).

56 Giles, A. J. *et al*. Dexamethasone-induced immunosuppression: mechanisms and implications for immunotherapy. *J Immunother Cancer* **6**, 51, doi:10.1186/s40425-018-0371-5 (2018).

57 Arbour, K. C. *et al*. Impact of Baseline Steroids on Efficacy of Programmed Cell Death-1 and Programmed Death-Ligand 1 Blockade in Patients With Non-Small-Cell Lung Cancer. *J Clin Oncol* **36**, 2872-2878, doi:10.1200/JCO.2018.79.0006 (2018).

58 Tokunaga, A. *et al*. Selective inhibition of low-affinity memory CD8(+) T cells by corticosteroids. *J Exp Med*, doi:10.1084/jem.20190738 (2019).

59 Wiedenheft, B. *et al*. Structures of the RNA-guided surveillance complex from a bacterial immune system. *Nature* **477**, 486-489, doi:10.1038/nature10402 (2011).

60 Hodgkins, A. *et al*. WGE: a CRISPR database for genome engineering. *Bioinformatics* **31**, 3078-3080, doi:10.1093/bioinformatics/btv308 (2015).

61 Pramanik, J. *et al*. Genome-wide analyses reveal the IRE1a-XBP1 pathway promotes T helper cell differentiation by resolving secretory stress and accelerating proliferation. *Genome Med* **10**, 76, doi:10.1186/s13073-018-0589-3 (2018).

# Figure 1

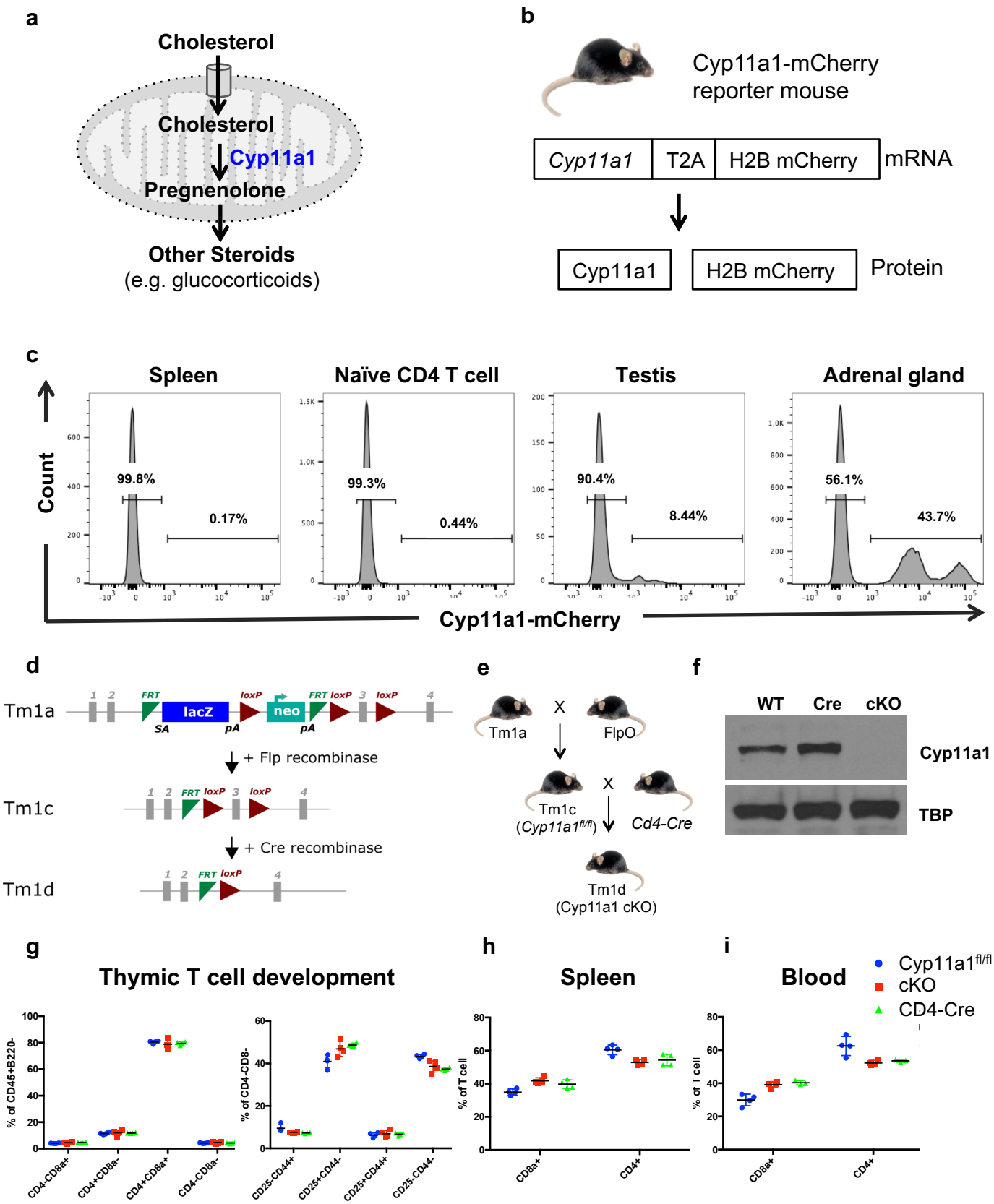
a
Cholesterol
Cholesterol
Cyp11a1
Pregnenolone
Other Steroids
(e.g. glucocorticoids)
b
Cyp11a1-mCherry
reporter mouse
Cyp11a1
T2A
H2B mCherry
mRNA
Cyp11a1
H2B mCherry
Protein
c
Spleen
Naïve CD4 T cell
Testis
Adrenal gland
Count
99.8%
0.17%
99.3%
0.44%
90.4%
8.44%
56.1%
43.7%
Cyp11a1-mCherry
d
Tm1a
FRT
lacZ
loxP
neo
FRT
loxP
SA
pA
pA
+ Flp recombinase
Tm1c
+ Cre recombinase
Tm1d
e
Tm1a
X
FlpO
Tm1c
(Cyp11a1fl/fl)
X
Cd4-Cre
Tm1d
(Cyp11a1 cKO)
f
WT
Cre
cKO
Cyp11a1
TBP
g
Thymic T cell development
% of CD45+B220-
% of CD4-CD8-
CD4-CD8a+
CD4+CD8a-
CD4+CD8a+
CD4-CD8a-
CD25-CD44+
CD25+CD44-
CD25+CD44+
CD25-CD44-
h
Spleen
% of T cell
CD8a+
CD4+
i
Blood
% of T cell
CD8a+
CD4+
Cyp11a1fl/fl
cKO
CD4-Cre

**Figure 1. Generation of a de novo steroidogenesis reporter and conditional knockout mice**

**a.** Schematic of de novo steroidogenesis pathway. In steroidogenic cells, such as testicular Leydig cells, cholesterol is imported into the mitochondria, where CYP11A1 converts it into pregnenolone, the first bioactive steroid of the pathway and precursor of all other steroids. CYP11A1 is the first and a key rate-limiting enzyme of the pathway.

**b.** Cyp11a1-mCherry reporter mice express H2B-tagged mCherry fluorescent protein, and Cyp11a1 as a single mRNA, driven by the endogenous Cyp11a1 promoter. The newly synthesized fusion protein self-cleaves due to presence of a T2A peptide and dissociates into two separate proteins: Cyp11a1 and H2B-mCherry.

**c.** Cyp11a1-mCherry reporter mice report Cyp11a1 expression accurately. Spleen, testis and adrenal glands were harvested from Cyp11a1-mCherry reporter mice. Tissues were mechanically dissociated and enzymatically digested into single cell suspension. Splenic naïve $CD4^+$ T cells were purified by using anti-CD4 antibody conjugated microbeads by using magnetic activated cell sorting (MACS). Single cell suspensions were analyzed by flow cytometry. Gating: All cells > Singlets > Live cells > Cyp11a1-mCherry. Representative of three independent experiments; each experiment contains 3-4 mice.

**d-e.** Generation of a Cyp11a1 conditional knockout mice. Schematic presentation of the Cyp11a1 conditional knockout mouse line and generation of T cell specific Cyp11a1 knockout mice (*Cd4*-Cre;*Cyp11a1*$^{fl/fl}$). The targeting allele is shown in (d) and the crossing strategy is on the (e).

**f.** Cyp11a1 knockout efficiency of Cre recombinase in T cells. Splenic naïve T helper cells from cKO (*Cd4*-Cre;Cyp11a1$^{fl/fl}$) mice or control mice (wild type and *Cd4*-Cre) were purified by negative selection using magnetic cell sorting, activated under Th2 differentiation condition, and analysed for Cyp11a1 protein expression by western blot.

**g.** Normal thymic development of T cells in Cyp11a1 cKO. Thymus was harvested from Cyp11a1 cKO and control (*Cd4*-Cre and Cyp11a1$^{fl/fl}$) mice, dissociated into single cell suspension, stained with fluorescent conjugated anti-CD4, CD8, B220, CD45, CD25 and CD44 antibodies, and analysed by flow cytometry. Gating: All cells > Singlets > Live cells >$CD45^+$ $B220^-$ > CD4, CD8 (left panel). $CD4^+CD8^+$ cells represent double positive (DP) stage, $CD4^+CD8^-$ and $CD4^-CD8^+$ cells represent single positive (SP) stage, $CD4^-CD8^-$ cells represent double negative (DN) stage. DN cells of the left panel were gated to show CD25 and CD44 expression to identify DN1 ($CD25^-CD44^+$), DN2 ($CD25^+CD44^+$), DN3 ($CD25^+CD44^-$) and DN4 ($CD25^-$ $CD44^-$).

**h-i.** Normal distribution of Cyp11a1 cKO T cells in the peripheral tissue. Blood and spleen were harvested from Cyp11a1 cKO and control (Cd4-Cre and Cyp11a1$^{fl/fl}$) mice, dissociated into single cell suspension, stained with fluorescent conjugated anti-CD4 and CD8 antibodies, and analysed by flow cytometry.

# Figure 2

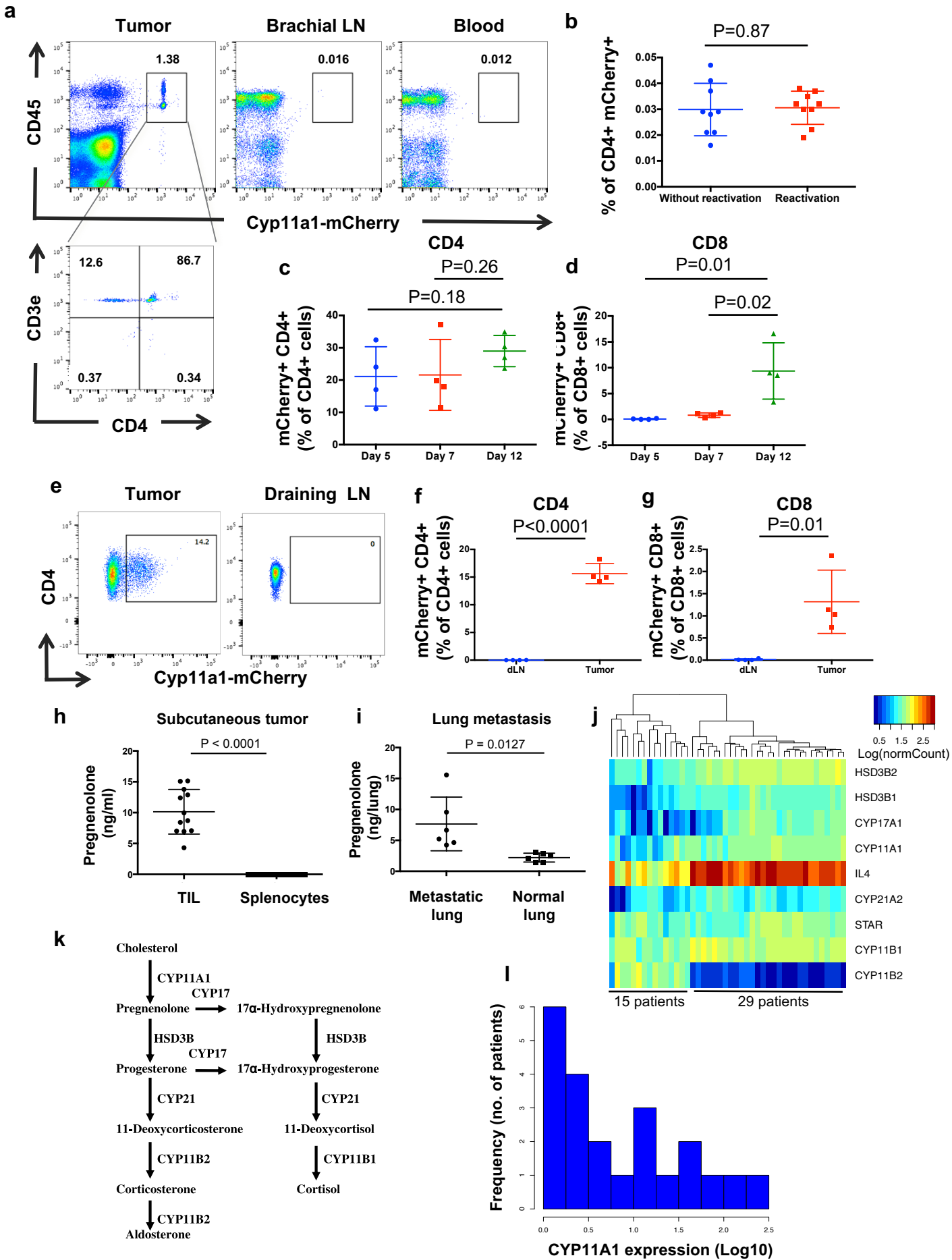
a
Tumor
Brachial LN
Blood
1.38
0.016
0.012
CD45
Cyp11a1-mCherry
12.6
86.7
0.37
0.34
CD3e
CD4
b
P=0.87
% of CD4+ mCherry+
Without reactivation
Reactivation
c
CD4
P=0.26
P=0.18
mCherry+ CD4+ (% of CD4+ cells)
Day 5
Day 7
Day 12
d
CD8
P=0.01
P=0.02
mCherry+ CD8+ (% of CD8+ cells)
e
Tumor
Draining LN
14.2
0
CD4
Cyp11a1-mCherry
f
CD4
P<0.0001
mCherry+ CD4+ (% of CD4+ cells)
dLN
Tumor
g
CD8
P=0.01
mCherry+ CD8+ (% of CD8+ cells)
h
Subcutaneous tumor
P < 0.0001
Pregnenolone (ng/ml)
TIL
Splenocytes
i
Lung metastasis
P = 0.0127
Pregnenolone (ng/lung)
Metastatic lung
Normal lung
j
Log(normCount)
HSD3B2
HSD3B1
CYP17A1
CYP11A1
IL4
CYP21A2
STAR
CYP11B1
CYP11B2
15 patients
29 patients
k
Cholesterol
CYP11A1
CYP17
Pregnenolone
17α-Hydroxypregnenolone
HSD3B
CYP17
HSD3B
Progesterone
17α-Hydroxyprogesterone
CYP21
CYP21
11-Deoxycorticosterone
11-Deoxycortisol
CYP11B2
CYP11B1
Corticosterone
Cortisol
CYP11B2
Aldosterone
l
Frequency (no. of patients)
CYP11A1 expression (Log10)

**Figure 2. Tumors induce Cyp11a1 expression in T cells in vivo**

**a.** Presence of steroidogenic (Cyp11a1$^{+}$) T cells in the B16-F10 melanoma tumor. B16-F10 cells were injected subcutaneously into the shoulder region of Cyp11a1-mCherry reporter mice. After 12 days brachial lymph node (LN), blood and tumor tissues were dissociated into single cell suspensions, and analyzed by flow cytometry. Gating strategy: Singlets > Live cells > CD45, Cyp11a1-mCherry. (N=5)

Cyp11a1 expression in CD4$^{+}$ T cells. CD45$^{+}$Cyp11a1-mCherry$^{+}$ cells were further gated to show T helper cell (CD4$^{+}$CD3e$^{+}$) expression of Cyp11a1.

**b.** In vitro restimulation of splenic T cells of tumor bearing mice does not induce Cyp11a1 expression. Splenic cells were purified from tumor bearing Cyp11a1-mCherry reporter mice, and reactivated/restimulated in vitro using PMA and ionomycin. Cyp11a1-mCherry expression in CD4$^{+}$ T cells was determined by flow cytometry. P-value was calculated using unpaired two-tailed t-test. Error bars represent mean ± s.d..

**c-d.** *In vivo* intratumoral Cyp11a1 expression dynamics in immune cells. B16-F10 cells were injected subcutaneously into the shoulder region of Cyp11a1-mCherry reporter mice. After 5, 7 and 12 days tumor tissues were dissociated into single cell suspensions, and analyzed by flow cytometry to detect the CD4$^{+}$ T cells (CD45$^{+}$Lin$^{-}$CD4$^{+}$CD3e$^{+}$CD8$^{-}$) (**c**), CD8$^{+}$ T cells (CD45$^{+}$Lin-CD8a$^{+}$CD3e$^{+}$CD4$^{-}$) (**d**)

**e-g.** Immune cell-mediated Cyp11a1 expression is conserved in EO771 orthotopic model of triple negative breast cancer. EO771 cells were injected into the mammary fat pad of Cyp11a1-mCherry reporter mice. After 15 days, tumor tissues and tumor draining LN were dissociated into single cell suspensions, and analyzed by flow cytometry to detect the Cyp11a1-mCherry expression in CD4$^{+}$ T cells (CD45$^{+}$Lin$^{-}$CD4$^{+}$CD3e$^{+}$CD8$^{-}$) (**e,f**), CD8$^{+}$ T cells (CD45$^{+}$Lin-CD8a$^{+}$CD3e$^{+}$CD4$^{-}$) (**g**)

**e.** Representative FACS profile of Cyp11a1$^{+}$CD4$^{+}$ T cells.

**f-g.** Representative graphical presentation of one experiment showing Cyp11a1 expressing CD4 and CD8 T cells.

**h-i. Tumors induce steroidogenesis in T cells *in vivo***

**h.** TIL supernatant contains pregnenolone. B16-F10 tumor-infiltrating leukocytes (TIL) were purified from tumor-bearing mice on post-inoculation day 12, cultured for 48 hours, and the supernatant was analyzed by ELISA to measure pregnenolone. Splenic leukocytes from the tumor bearing mice were used as control. N=12, pooled analysis of three independent experiments, symbol represents individual mouse, error bars represent mean ± s.e.m., unpaired two-tailed t-test.

**i.** Metastatic dissemination of cancer cells induces steroid biosynthesis. Metastasized lungs were harvested 10 days post-B16-F10 intravenous injection in C57BL/6 mice, dissociated into single cell suspension, cultured for 48 hours and the supernatant was analyzed by ELISA. Naïve uninfected lungs (normal lung) were used as control. N=6, symbol represents individual mouse, pooled analysis of two independent experiments, error bars represent mean ± s.e.m., unpaired two-tailed t-test.

**j**. Human tumors induce de novo steroidogenesis. Steroidogenic gene expression is correlated with IL4 expression in human melanoma. Hierarchical clustering of steroidogenic genes and IL4 mRNA expression across 44 melanoma patient samples (Raw data source: GEO: GSE19234).

**k**. Schematics showing glucocorticoids (corticosterone and cortisol) synthesis pathway.

**l.** Frequency distribution histogram showing CYP11A1 mRNA expression (normalized read counts, log10 scale) across 22 melanoma patients' tumor infiltrating CD4$^{+}$ T cells (Raw data accession code EGAD00001000325).

# Figure 3

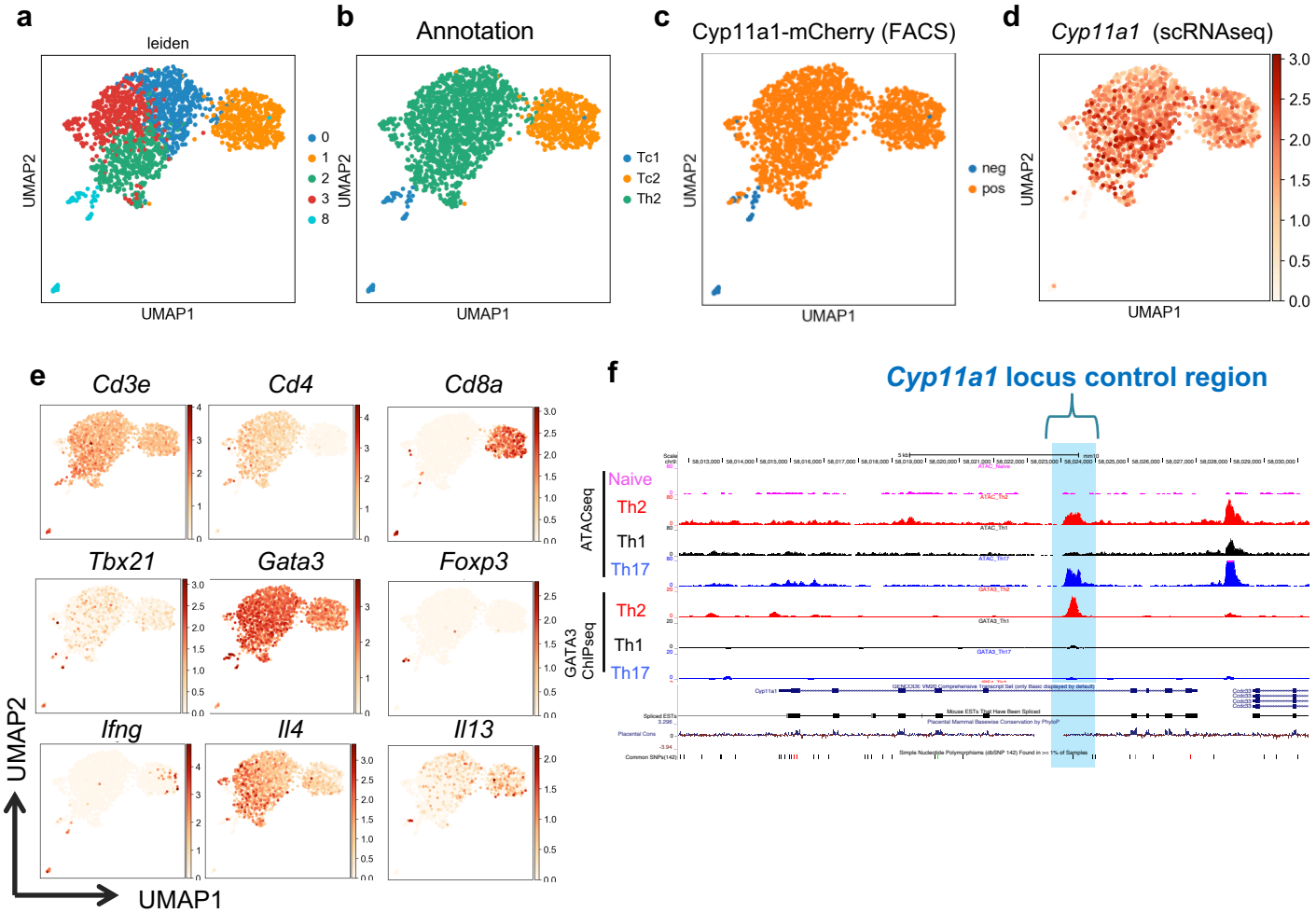
a
leiden
0
1
2
3
8
UMAP2
UMAP1
b
Annotation
Tc1
Tc2
Th2
UMAP2
UMAP1
c
Cyp11a1-mCherry (FACS)
neg
pos
UMAP2
UMAP1
d
Cyp11a1 (scRNAseq)
UMAP2
UMAP1
e
Cd3e
Cd4
Cd8a
Tbx21
Gata3
Foxp3
Ifng
Il4
Il13
UMAP2
UMAP1
f
Cyp11a1 locus control region
ATACseq
Naive
Th2
Th1
Th17
GATA3 ChIPseq
Th2
Th1
Th17

**Figure 3. Single-cell transcriptomics revealed gene expression identity and gene expression pattern of intratumoral steroidogenic T cells**

**a,b.** UMAP visualization of the tumor infiltrating T cells (a) with annotations of the clusters (b). Tc1 represents type-1 $CD8^+$ T cells, Tc2 represents type-2 $CD8^+$ T cells and Th2 represents type-2 $CD4^+$ T cells.

**c,d.** mCherry protein expression perfectly reports *Cyp11a1* mRNA expression. Cyp11a1-mCherry protein expression according to the FACS data (c). *Cyp11a1* mRNA expression in the scRNA-seq data (d).

**e.** Expression of cell type specific signature genes that were used to annotate the clusters.

**f.** Determination of *Cyp11a1* locus control region. Open chromatin regions were identified by ATAC-seq of T helper cells. In vitro generated Th2 and Th17 cells were used as positive control. Naïve and Th1 cells were used as negative control. Gata3 ChIP-seq data were analyzed to determine the binding site. The open chromatin region where Gata3 occupy is highlighted blue and considered as locus control region.

# Figure 4

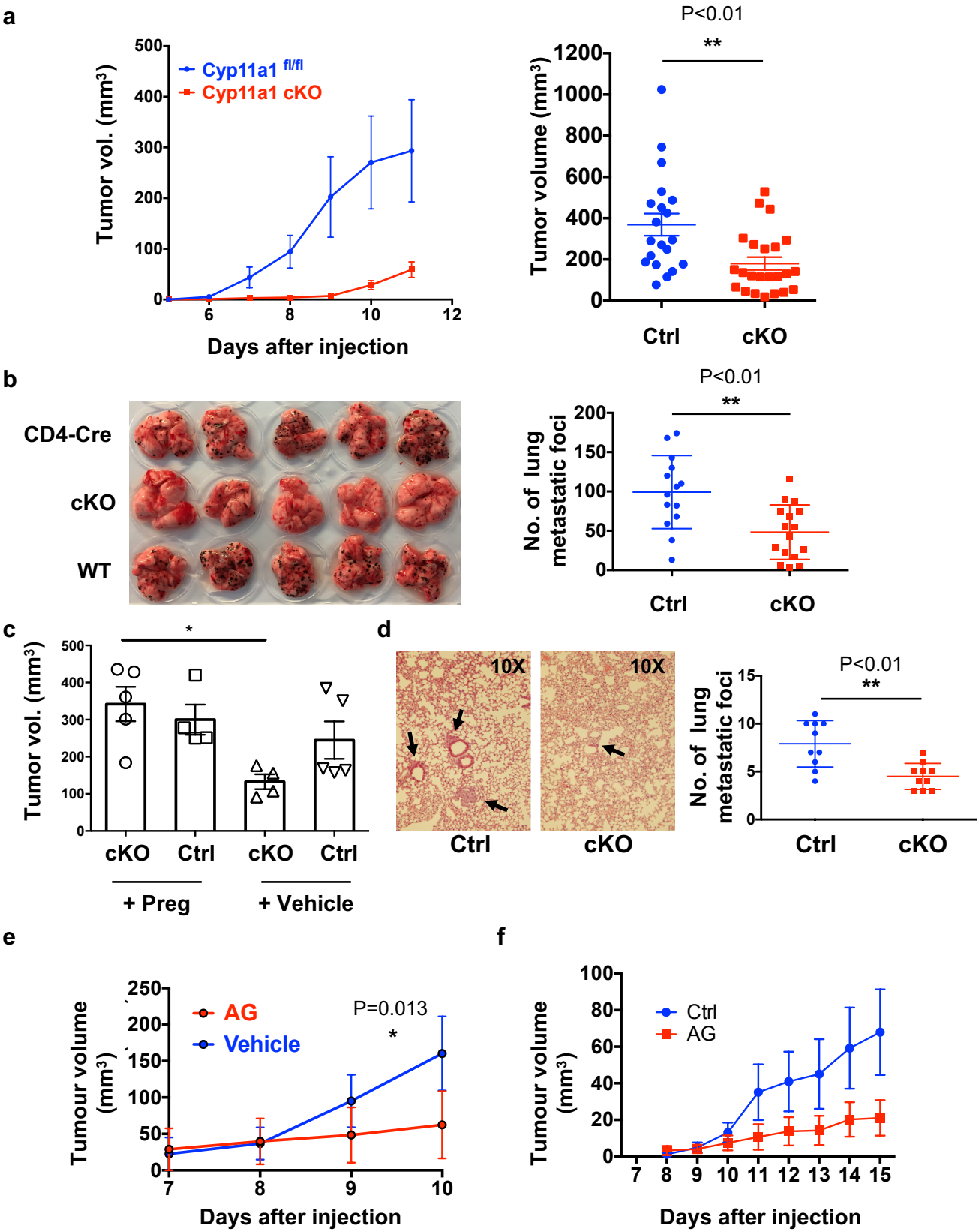
a
Cyp11a1 fl/fl
Cyp11a1 cKO
Tumor vol. (mm³)
Days after injection
P<0.01
**
Tumor volume (mm³)
Ctrl
cKO
b
CD4-Cre
cKO
WT
P<0.01
**
No. of lung metastatic foci
Ctrl
cKO
c
*
Tumor vol. (mm³)
cKO
Ctrl
cKO
Ctrl
+ Preg
+ Vehicle
d
10X
10X
Ctrl
cKO
P<0.01
**
No. of lung metastatic foci
Ctrl
cKO
e
AG
Vehicle
P=0.013
*
Tumour volume (mm³)
Days after injection
f
Ctrl
AG
Tumour volume (mm³)
Days after injection

**Figure 4. Ablation of T cell de novo steroidogenesis restricts experimental tumor growth and metastasis**

**a.** Genetic deletion of Cyp11a1 in T cells inhibits primary tumor growth of B16-F10 melanoma cells. Left-panel: B16-F10 subcutaneous tumor growth curve assessed in T cell specific Cyp11a1 cKO (cKO) and Cd4-Cre control mice (n=5, representative of four independent experiments, error bars represent mean ± s.e.m.). Tumors were measured every day from 6th day after subcutaneous injection of B16-F10 cells. Right panel: Graphical presentation of end-point tumor volume ($n \geq 20$, pooled data of four independent experiments, error bars represent mean ± s.e.m., unpaired two-tailed t-test).

**b.** Genetic deletion of Cyp11a1 in T cells inhibits experimental lung metastasis of B16-F10 melanoma. Left panel: Representative photograph of pulmonary metastatic foci produced 10 days after tail vein injection of B16-F10 cells. Right panel: Graphical presentation of the numbers of lung metastatic foci (right panel) ($n \geq 15$, pooled data of three independent experiments, error bars represent mean ± s.d., unpaired two-tailed t-test).

**c.** Pregnenolone complements the Cyp11a1 deficiency in Cyp11a1 cKO mice. Cyp11a1 cKO and Cd4-Cre control mice were injected with B16-F10 cells. Pregnenolone or vehicle (DMSO) applied topically at the primary tumor site every 48 hrs. Tumor volume was measured at the end-point at day 12. N=5, error bars represent mean ± s.e.m., one way ANOVA, representative experiment.

**d.** Genetic deletion of *Cyp11a1* in T cells inhibits experimental lung metastasis of EO771 breast cancer cells. Representative hematoxylin and eosin stained histologic photograph of pulmonary metastatic foci produced 10 days after tail vein injection of EO771 cells in Cyp11a1 cKO and $Cyp11a1^{fl/fl}$ mice. Graphical presentation of the numbers of lung metastatic foci (right panel).

**e.** Cyp11a1 inhibitor aminoglutethimide restricts melanoma tumor growth. B16-F10 cells were injected subcutaneously in C57BL/6 mice with or without Cyp11a1 inhibitor aminoglutethimide (AG). AG treatment was continued with a 48 hrs interval (N=5, error bars represent mean ± s.e.m, two way ANOVA, P=0.013, representative experiment).

**f.** Cyp11a1 inhibitor aminoglutethimide restricts orthotopic breast cancer growth. EO771 cells were injected into the mammary fat pad in C57BL/6 mice with or without Cyp11a1 inhibitor AG. AG treatment was continued with a 48 hrs interval. (N=5, error bars represent mean ± s.e.m., representative experiment).

# Figure 5

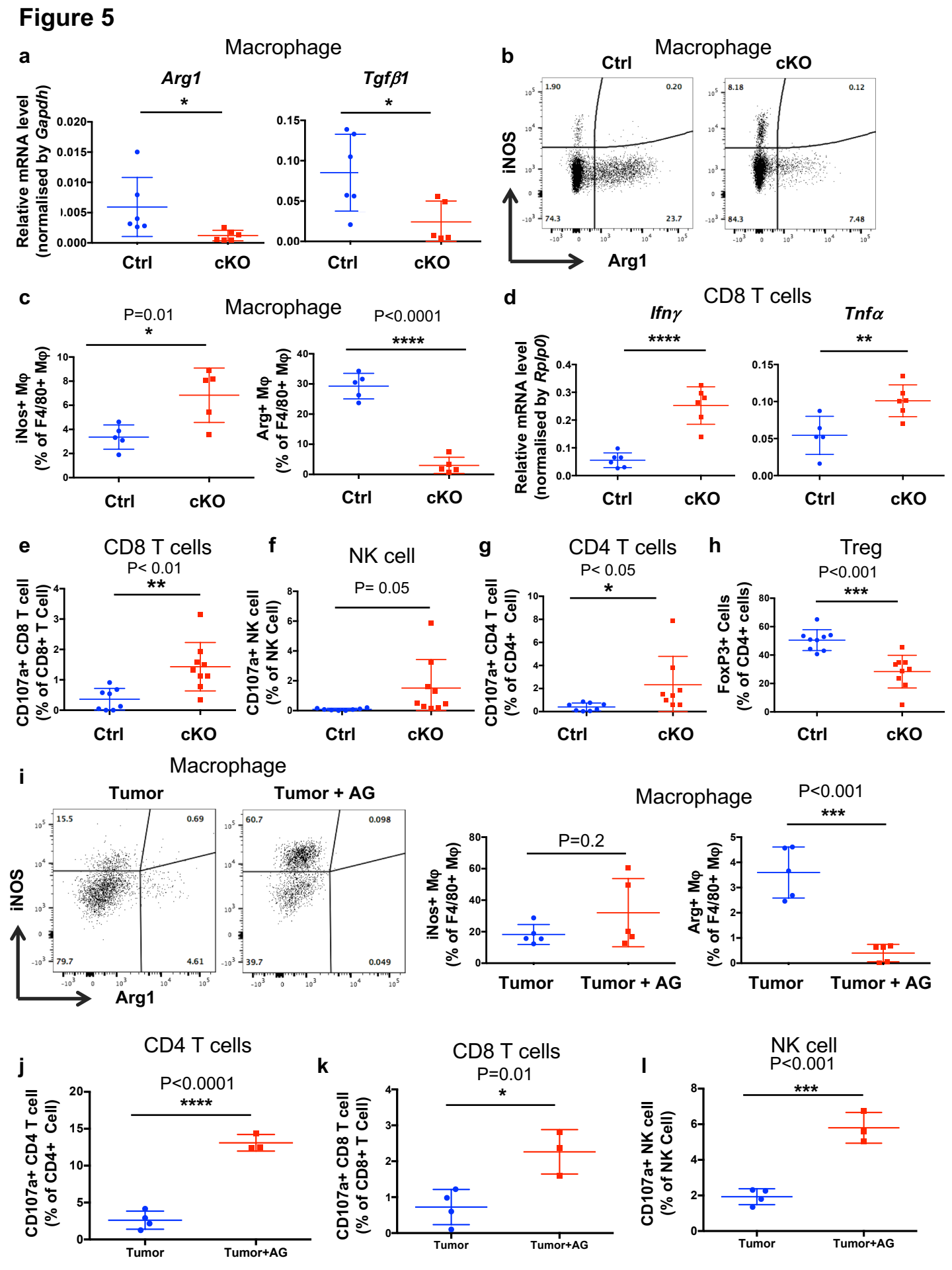
a
Macrophage
Arg1
Tgfβ1
Relative mRNA level (normalised by Gapdh)
Ctrl
cKO
b
Macrophage
Ctrl
cKO
iNOS
Arg1
1.90
0.20
74.3
23.7
8.18
0.12
84.3
7.48
c
Macrophage
P=0.01
P<0.0001
iNos+ Mφ (% of F4/80+ Mφ)
Arg+ Mφ (% of F4/80+ Mφ)
d
CD8 T cells
Ifnγ
Tnfα
Relative mRNA level (normalised by Rplp0)
e
CD8 T cells
P< 0.01
CD107a+ CD8 T cell (% of CD8+ T Cell)
f
NK cell
P= 0.05
CD107a+ NK cell (% of NK Cell)
g
CD4 T cells
P< 0.05
CD107a+ CD4 T cell (% of CD4+ Cell)
h
Treg
P<0.001
FoxP3+ Cells (% of CD4+ cells)
i
Macrophage
Tumor
Tumor + AG
iNOS
Arg1
15.5
0.69
79.7
4.61
60.7
0.098
39.7
0.049
Macrophage
P=0.2
P<0.001
iNos+ Mφ (% of F4/80+ Mφ)
Arg+ Mφ (% of F4/80+ Mφ)
j
CD4 T cells
P<0.0001
CD107a+ CD4 T cell (% of CD4+ Cell)
Tumor
Tumor+AG
k
CD8 T cells
P=0.01
CD107a+ CD8 T cell (% of CD8+ T Cell)
l
NK cell
P<0.001
CD107a+ NK cell (% of NK Cell)

**Figure 5. Inhibition of T cell steroidogenesis stimulates anti-tumor immunity.**

**a-h**. Comparing Cyp11a1 cKO and *Cd4*-Cre control mice with B16-F10 cells injected subcutaneously (n= 5 or 6, error bars represent mean ± s.d., unpaired two-tailed t-test, representative experiment).

**a.** Tumor infiltrating macrophages (Lin-CD11b$^+$) were purified by cell sorting at day 12. *Arg1* and *Tgfb1* mRNA expression was quantified by RT-qPCR, with mRNA expression level normalized by *Gapdh* mRNA expression.

**b-c.** Tumor infiltrating macrophages (Lin$^-$CD11b$^+$F4/80$^+$) analyzed by flow cytometry at day 12 to examine iNOS and Arg1 expression. Representative FACS profile of the expression (b). Representative graphical representation of one experiment (n = 5).

**d.** Tumor infiltrating CD3e$^+$CD8$^+$ T cells purified by cell sorting at day 12, reactivated ex vivo, and *Ifng* and *Tnfa* mRNA expression quantified by RT-qPCR, with mRNA expression level was normalised by *Rplp0* expression.

**e.** Cytotoxic T lymphocyte (CD8$^+$ T cell) degranulation assay. CD107a/LAMP1 expression on tumor infiltrating CD8$^+$ T cells was analyzed by flow cytometry after 12 days post-inoculation of B16-F10 cells. Gating: All cells > singlets > live cells > CD8$^+$ T cell > CD107a.

**f.** NK cell degranulation assay by measuring CD107a/LAMP1 expression on tumor infiltrating NK cells. Gating: All cells > singlets > live cells > NK cells > CD107a.

**g.** CD4$^+$ T cell degranulation assay by measuring CD107a/LAMP1 expression on CD4$^+$ T cells. Gating: All cells > singlets > live cells > CD4$^+$ T cell > CD107a

**h.** Number of regulatory T cells in the TME decreases upon Cyp11a1 deletion. Flow cytometric analysis to show the changes in B16-F10 subcutaneous tumor infiltrating Treg (CD4$^+$CD3e$^+$FoxP3$^+$) population upon Cyp11a1 deletion.

**i-l.** Comparing immunophenotype in Cyp11a1 inhibitor, AG, treated and untreated mice with B16-F10 cells injected subcutaneously (n= 5 or 6, error bars represent mean ± s.d., unpaired two-tailed t-test, representative experiment)., representative experiment).

**i.** Representative FACS profile to show iNOS and Arg1 expression in tumor infiltrating CD45$^+$Lin$^-$ CD11b$^+$F4/80$^+$ macrophages (left panel). Graphical presentation the iNOS and Arg1 expression of a representative experiment (right panel).

**j.** CD4$^+$ T cell degranulation assay by measuring CD107a/LAMP1 expression on CD4$^+$ T cells. Gating: All cells > singlets > live cells > CD4$^+$ T cell > CD107a.

**k.** Cytotoxic T lymphocyte (CD8$^+$ T cell) degranulation assay. CD107a/LAMP1 expression on tumor infiltrating CD8$^+$ T cells was analyzed by flow cytometry after 12 days post-inoculation of B16-F10 cells. Gating: All cells > singlets > live cells > CD8$^+$ T cell > CD107a.

**l.** NK cell degranulation assay by measuring CD107a/LAMP1 expression on tumor infiltrating NK cells. Gating: All cells > singlets > live cells > NK cells > CD107a.

# Figure 6

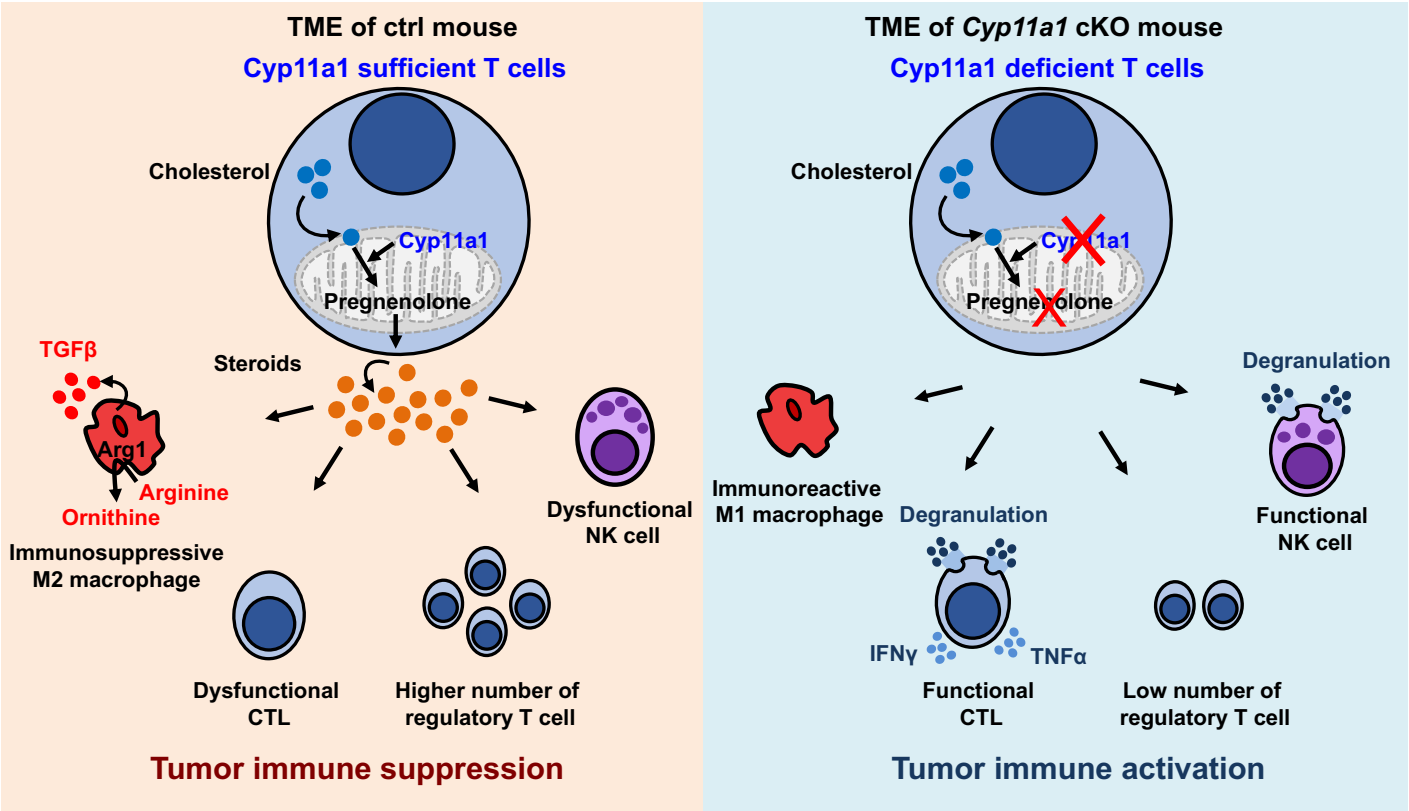
TME of ctrl mouse
Cyp11a1 sufficient T cells
Cholesterol
Cyp11a1
Pregnenolone
Steroids
TGFβ
Arg1
Arginine
Ornithine
Immunosuppressive
M2 macrophage
Dysfunctional
NK cell
Dysfunctional
CTL
Higher number of
regulatory T cell
Tumor immune suppression
TME of Cyp11a1 cKO mouse
Cyp11a1 deficient T cells
Cholesterol
Cyp11a1
Pregnenolone
Degranulation
Immunoreactive
M1 macrophage
Degranulation
Functional
NK cell
IFNγ
TNFα
Functional
CTL
Low number of
regulatory T cell
Tumor immune activation

**Figure 6. Graphical abstract of the discovery.**

T cell mediated de novo steroidogenesis in the tumor microenvironment promotes tumor growth by inhibiting anti-tumour immunity, in part by inducing M2 phenotype in macrophages and suppressing T and NK cell function. Genetic deletion of Cyp11a1 or pharmacologic inhibition of Cyp11a1 activity stimulates anti-tumor immunity by increasing the number of M1 macrophages, functional T cells and decreasing the number of regulatory T cells, M2 macrophages.